



HAL
open science

Design and Development of Single-Qubit Ion Trap on Glass and Si Substrates With RF Analysis and Performance Benchmarking

Anak Agung Alit Apriyana, Hongyu Li, Peng Zhao, Jing Tao, Yu Dian Lim, Ye Lin, Luca Guidoni, Chuan Seng Tan

► **To cite this version:**

Anak Agung Alit Apriyana, Hongyu Li, Peng Zhao, Jing Tao, Yu Dian Lim, et al.. Design and Development of Single-Qubit Ion Trap on Glass and Si Substrates With RF Analysis and Performance Benchmarking. IEEE Transactions on Components, Packaging and Manufacturing Technology, 2020, 10 (7), pp.1221-1231. 10.1109/TCPMT.2020.2995388 . hal-03066791

HAL Id: hal-03066791

<https://hal.science/hal-03066791>

Submitted on 15 Dec 2020

HAL is a multi-disciplinary open access archive for the deposit and dissemination of scientific research documents, whether they are published or not. The documents may come from teaching and research institutions in France or abroad, or from public or private research centers.

L'archive ouverte pluridisciplinaire **HAL**, est destinée au dépôt et à la diffusion de documents scientifiques de niveau recherche, publiés ou non, émanant des établissements d'enseignement et de recherche français ou étrangers, des laboratoires publics ou privés.

Design and Development of Single Qubit Ion-Trap on Glass and Si Substrates with RF Analysis and Performance Benchmarking

Anak Agung Alit Apriyana*, *Member, IEEE*, Hong Yu Li*, Peng Zhao*, Jing Tao*, Yu Dian Lim, Ye Lin, Luca Guidoni, and Chuan Seng Tan, *Senior Member, IEEE*

Abstract—This study presents the design and development of surface electrode ion traps on glass and Si substrate, as well as their RF characterizations and performance benchmarking. In this case, ion-trap on-glass shows superior performances in all necessary criteria. In terms of RF characterizations, ion-traps on glass have Q factor of greater than 900. This is significantly higher than the Q factor of its silicon counterparts, which are around 20 – 300. Such a high Q factor results in power spectral density (PSD) of greater than 10W/MHz. On the other hand, ion-traps on-silicon produce PSD values of lower than 3W/MHz. In terms of RF performance, ion-trap on-glass shows insertion loss lower than 0.2 dB at 60MHz. This is more superior to insertion loss values of ion-traps on-silicon, which are around 1 – 4 dB. The ion-traps metallization is developed using three metallization layers (0.1 μ m Ti barrier layer, 2.5 – 3.7 μ m Cu, and 0.3 μ m Au) on top of dielectric. The on-chip resonance condition can be maintained upon the packaging integration. The laser optical setup for ion-trapping is verified to capture single $^{88}\text{Sr}^+$ ion.

Index Terms—Ion-trap, power spectral density, power dissipation, RF analysis, microfabrication, IC packaging, laser excitation, qubit operation

I. INTRODUCTION

QUANTUM computing is the computation systems that use quantum-mechanical phenomena (e.g. superposition, entanglement) to perform the computing operation, instead of the conventional Boolean logic by its classical computing counterparts. Quantum computation uses quantum bits, i.e. qubits, to represent ‘1’ and ‘0’ states simultaneously, solving large-scale computation (i.e., chemical simulation, large number factoring and travel salesman problem), which are intractable for classical computer [1]. Superconducting loops, trapped ion, polarized photon, quantum dot and spinning atom can be used as physical implementations for

qubit. Qubit that is based on trapped ion receives more attention recently due to its high efficiency and feasibility of large-scale planar ion-trap electrodes implementation using microfabrication process. With the combination of electric field (E-field) induced by co-planar radio frequency (RF) and direct current (DC) electrodes placed on the same plane, a localized minimum potential point will be formed above the surface, where ion will be trapped. Lasers with specific wavelengths will be exerted onto ions for cooling, state readout and manipulation.

Two states (ground state and excited state) of the valence energy levels in the trapped ions are used to represent logic ‘0’ and ‘1’ of the qubit. Qubit operation can be performed to the trapped ions using a series of laser excitations to induce the laser-atom interactions for inter-state electrons transitions from the ground state to the excited state. When an electron in the ground state (logic ‘0’) is excited with an appropriate laser wavelength, the electron can be excited to higher energy level (logic ‘1’). For logic ‘1’ to logic ‘0’ transition, another laser beam will be required to further excite the electron into the transition states that will spontaneously decay back into the ground state. Depending on the ion lifetime, multiple cycles of this electron transition can be repeated to perform the quantum gate operations [1].

In surface electrode ion-trap design, the typical ‘five-wire’ geometry (control, RF, ground, RF and control) is employed, which consists of two parallel RF electrodes and one ground electrode sandwiched in between forming RF-G-RF lines. Segmented DC electrodes are placed next to each RF electrode, to control the ions position along axial (Z) direction and shuttle ions to certain sites (if necessary), as shown in Fig.1. Ion trap requires RF sources for E -field excitation, and the excited E -field will form the pseudopotential for ion trapping. The ion trapping performance is influenced by the strength of the applied E -field, where stronger E -field produces higher trapping potential, resulting in higher stability of the trapped ion.

Glass has been reported as a candidate substrate for the development of surface electrode ion-trap due to its excellent electrical properties including ultra-high substrate resistivity, low dielectric constant, and ultra-low electrical loss. These properties result in efficient current-to- E -field conversion for the formation of ion-trapping pseudopotential. Efficient current-to- E -field conversion is also crucial in preventing heat generation under the application of RF potential, where the conventional magnitude of RF voltage required for ion trapping can be as high as 100 – 500Vpp. On the other hand,

This document is submitted on 30 May 2019. The work was supported by A*STAR Quantum Technology for Engineering (A1685b0005).

*The first four authors contributed equally to this work.

A.A.A Apriyana, P. Zhao, J. Tao, Y. D. Lim, Y. Lin and C. S. Tan are with Nanyang Technological University, 50 Nanyang Avenue Singapore 639798. (E-mail: aapriyana@ntu.edu.sg, zhao0275@e.ntu.edu.sg, taojing@ntu.edu.sg, yudian.lim@ntu.edu.sg and tancs@ntu.edu.sg).

H. Y. Li is with Institute of Microelectronics, Agency for Science, Technology and Research (A*STAR), Singapore 117685. (email: lihy@ime.a-star.edu.sg)

L. Guidoni is with Laboratoire Matériaux et Phénomènes Quantiques (MPQ), Université Paris, France F-75205 (email: luca.guidoni@univ-paris-diderot.fr).

as compared to Si substrate, back-grinding, and polishing process required can be avoided in glass substrate due to its scalable thickness (down to 100 μm) [2]. Possibilities to fabricate blind-vias and through glass vias (TGV) further extends the benefit of glass substrate for ion-trap implementation [3], as 3D integration with TGV and multi-layer metallization option are essential features in multi-qubits quantum computing system, where up to thousands of RF and DC electrodes are required. Besides, by adjusting their coefficient of thermal expansion (CTE) to be close or even equal to Si substrate [4], the ion trap on glass can also be integrated into silicon substrate to combine the high-performance ion trap on-glass with other Si-circuit building blocks such as digital-to-analog converter, voltage regulator, low-pass filter, RF source, etc. to obtain full system integration. Such hetero-structure ion-trap design had been reported in [5].

Besides glass substrates, silicon substrates have also been explored in ion trap implementation for their CMOS-compatible fabrication process and high density integration technologies such as the through silicon via (TSV) interconnection and multilayer metallization, which are particularly useful for multi-qubits quantum computing system [6]-[12]. However, the high RF loss of Si hinders its feasibility in full-silicon integrated ion trap system scheme [13]-[18]. Some possible solutions have been proposed, such as the introduction of grounding layer, increasing the insulation layer (SiO_2) thickness (up to 10 μm), lowering the work temperature (<10K), etc. In our design, by utilizing high resistivity silicon substrate (> 750 Ωcm), both leakage current and loss tangent of silicon substrate can be reduced. Therefore, a favorable RF performance is expected.

In order to characterize their performance difference, we developed both ion-traps on glass and Si substrate with identical design geometry. Corresponding RF analysis and characterization as well as performance benchmarking are presented. The on-chip performances such as the insertion loss, capacitance stability, Q factor, power efficiency, power spectral density, power dissipation are tabulated for comparison. We have also integrated the chips into the standard CPGA packaging to verify their on-package performances. The final verifications are ion trapping testing by laser optical set-up in ultra-vacuum environment. In this case, the designed ion trap on glass successfully confines ion with lifetime tens of minutes under 110V_{pp} and 39 MHz of RF excitation.

This study begins with the overview of the fundamentals of quantum computing and surface electrode ion-trap implementation on glass and Si substrate in Section I. Next, RF analysis is presented in Section II and ion-trap resonance characterization is elaborated in Section III. After that, the microfabrication process of the ion-traps is presented in Section IV, where the integration of fabricated traps into the CPGA packaging is discussed in Section V. Section VI shows the optical measurement set-up that has successfully captured single $^{88}\text{Sr}^+$ ion. Lastly, the key findings are concluded in Section VII.

II. RF CHARACTERIZATION

TABLE I
THE SUBSTRATE PROPERTIES FOR ION-TRAP CHARACTERIZATION

Substrate type	Electrical resistivity ($\Omega\cdot\text{cm}$) @ RT	Dielectric Loss Tangent, $\tan \delta$	Use condition for ion trapping	Microfabrication compatibility
Low resistivity Si (LRSi)	1-10	> 1.5 @ 20MHz	Lossy substrate (highly-doped Si)	Standard substrate, CMOS-compatible
High resistivity Si (HRSi)	> 750	\sim 1.5 @ 20MHz	Low-loss substrate	Standard substrate, CMOS-compatible
Glass	\sim 10 ¹⁰	0.025 @ 5 GHz	Lossless substrate	New substrate for wafer fabrication

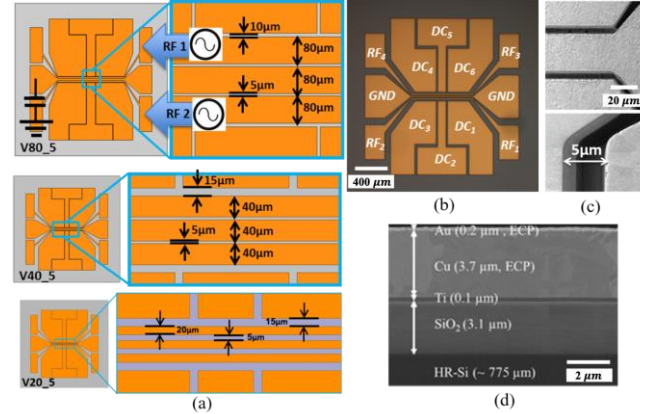


Fig.1. The ion-trap test vehicles with RF and DC biasing set-up and metal layers structural composition. (a) The three variations of design vehicles (V20_5, V40_5, and V80_5) with their respective RF and GND lines dimensions. Version V80_5 has the line width of 80 μm while the smallest version V20_5 has line width of 20 μm . (b) The biasing set-up for the ion trap that consists of RF excitation, central GND and DC biases & (c) The SEM picture of die with the metallization spacing measurement. (d) The cross-section of die photo which shows the actual built of metallization thickness (Ti-Cu-Au) layers.

TABLE II
THE DIMENSION OF RF ELECTRODES OF THE DESIGN VEHICLES

Design vehicles	Dimension of RF electrodes (G-S-G) lines			Chip area $L \times W$ (mm^2)
	RF line width (μm)	Spacing (μm)	Length (μm)	
V20_5	20	5	730	1.8 \times 1.8 (3.24)
V40_5	40	5	1460	3.9 \times 3.9 (14.90)
V80_5	80	5	2920	7.9 \times 7.9 (62.4)

Fig. 1 shows planar surface-electrode ion-trap designs with three design variations (V20_5, V40_5, and V80_5), which are used to characterize the insertion losses, capacitances and also the Q factors of the ion-traps due to devices scaling and substrate variations. Their associated dimensions are given by Table II. Each of ion-trap design on Si substrate has similar metallization layers composition, which consists of three sandwiched metallization layers (Ti (0.1 μm), Cu (3.7 μm), and Au (0.2 μm)) on top of silicon dioxide. The main differences among the test vehicles are the width and length of the RF and ground lines. Upon the application of RF signal, electric field

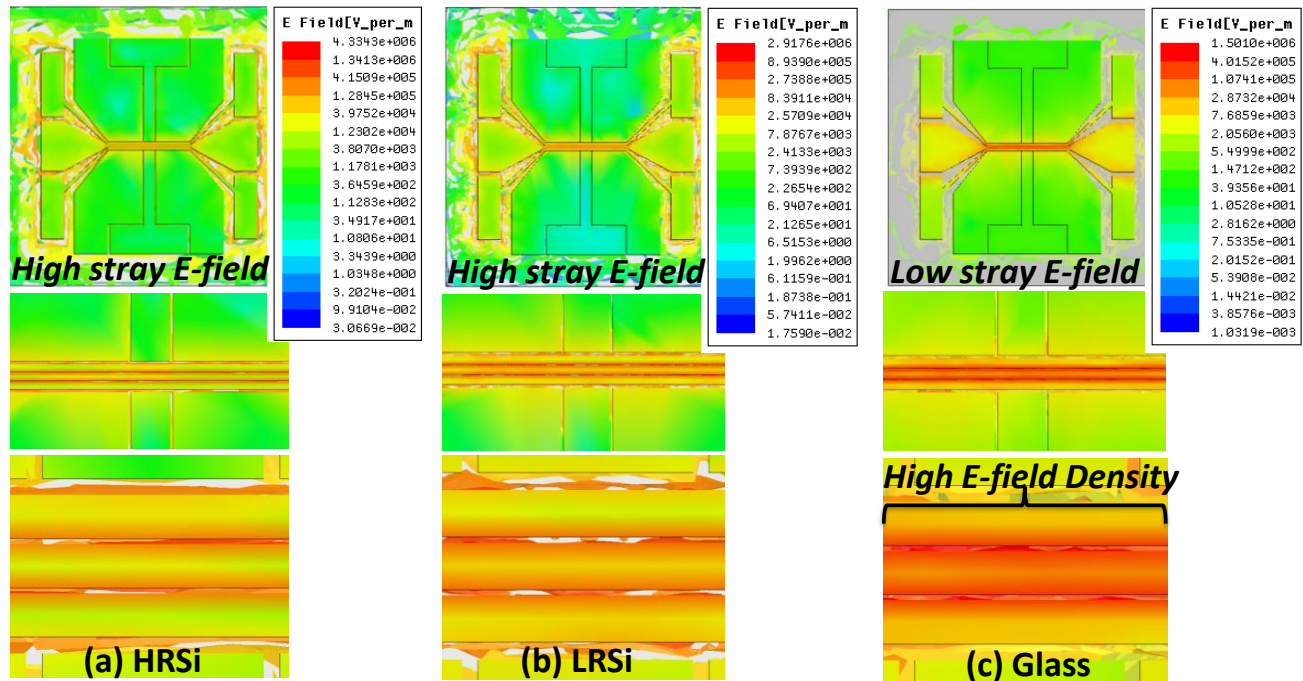


Fig.2. Comparison of E -field characteristic of RF-excited ion-traps on HRSi, LRSi and glass at 60MHz. (a) and (b) E -field on HRSi and LRSi respectively, with high stray E -field on exposed oxide layer. (c) The E -field characteristic of ion trap-on-glass with low stray E -field but high E -field density around the trapping zone.

(E -field) will be excited from RF lines and terminated into the ground line for the formation of pseudopotential.

Fig.2 shows the E -field characteristic distributions of the ion-traps test vehicles on high resistivity silicon (HRSi), low resistivity silicon (LRSi) and glass respectively. As shown in Fig.2(a) and (b), both ion-traps designs on HRSi and LRSi produce high stray E -field (in the order of $10^3 - 10^4$ V/m) as observed around the exposed dielectric area (non-metallized area). These amounts of stray E -field increase power dissipation and parasitic capacitance, which lead to higher resonance loss and lower Q factor [19]. Subsequently, lower Q value increases the power bandwidth and reduces the power spectral density (PSD) [20]. The reduction in power spectral density indicates that more power is needed to be delivered to the ion trap to form the pseudopotential. Hence, the end product of this stray of E -field is in the form of heat dissipation which affects the overall operation of the quantum computing system.

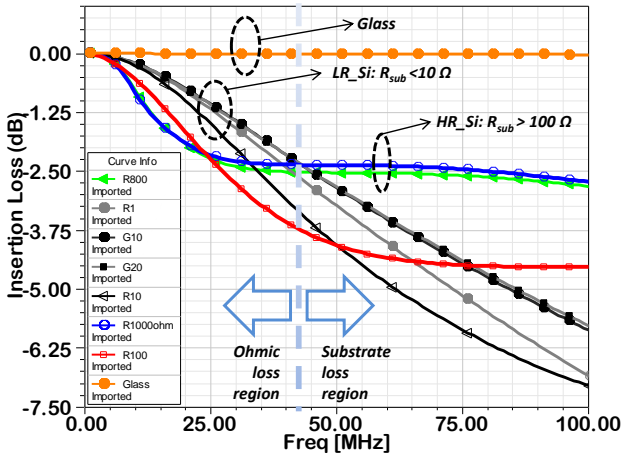
On the other hand, the E -field distribution of ion-trap on-glass shows higher density around the central lines (in the area around the two RF lines that sandwich the ground line). The stray E -field around the exposed substrate is also showing lower density than the observation on HRSi and LRSi. Based on this E -field quality, ion-trap on-glass is expected to have higher quality factor, lower power dissipation, and higher power spectral density.

Fig.3 demonstrates the superiority of ion-traps on-glass in terms of RF performances as compared to their Si counterparts, which are highly dependent on Si substrate conductivity. As the substrate resistivity increases, the insertion loss increases at low frequency region but improves at high frequency region. This can be attributed to the dominance of Ohmic loss at low frequency; while substrate

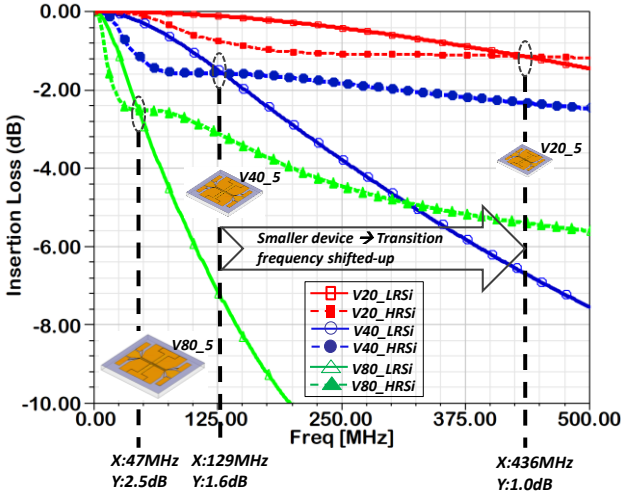
loss is dominant at high frequency. Between these frequency regions, a transition frequency exists, which is defined as the frequency point where the effect of Ohmic loss is equal to the substrate loss.

The insertion loss of the ion-trap on glass is around 0.2dB, which is far more superior to the ion-trap performances on any variation of substrate conductivity of Si substrate. This is also confirmed by the measurement results as given by Fig.4. Fig. 3(b) shows the shift in transition frequency due to device scaling. Overall, the high resistivity Si substrate (HRSi) gives better insertion loss performance than low resistivity Si substrate (LRSi) at frequency higher than transition frequency. Understanding this substrate conductivity related behavior is very critical in choosing which Si substrate is more appropriate for certain ion-trap design dimension.

In order to choose which silicon substrate resistivity will give better performance, we need to map the transition frequencies of the substrates with respect to the resonance frequency as given by Fig.3 (a). When the resonance frequency is set to be equal to 75MHz (higher than transition frequency (43MHz)); the high resistivity silicon substrates have better insertion loss than low resistivity substrates. However, if the resonance frequency is set to be equal to 25MHz (lower than transition frequency (43MHz)); the lower resistivity substrates have better insertion loss than high resistivity substrate. Therefore, the choice of silicon substrate resistivity is fundamentally determined by the applied RF excitation frequency and relative position of transition frequency with respect to the resonance frequency.



(a)



(b)

Fig.3. The ion-trap on glass superior insertion loss performance compared to Si counterparts and the transition frequency defining the frequency range of Ohmic loss region or substrate loss region of silicon substrate. (a) Change in insertion losses due to variation in substrate conductivities with distinction in glass performance. (b) Shift-up in transition frequency due to device scaling of ion-traps on Si substrate.

III. RESONANCE CHARACTERISTIC

A. Equivalent Capacitance & Q Factor

Ion trap is a capacitive device and its capacitance is built by E -field excitation. The E -field fluxes are coming out from the pair of RF lines and terminate themselves into the central ground lines. Assuming the phases of RF signal sources into the RF lines are perfectly balanced, there will be E -field cancellation along the axial confinement (axis of central ground lines). Depending on the width and spacing between RF and central ground lines, the pseudopotential will be zero at certain height above axial confinement and maximum in the area between the RF line and ground line. The potential difference between the minimum (zero level) and maximum defines the height of trapping potential (meV), which correlates to the kinetic energy needed by the trapped ions to escape from this trapping potential.

The profile of the pseudo-potential is reflected into the equivalent capacitance of the ion-trap. Uniform pseudo-potential along the axis of confinement is indicated by stable

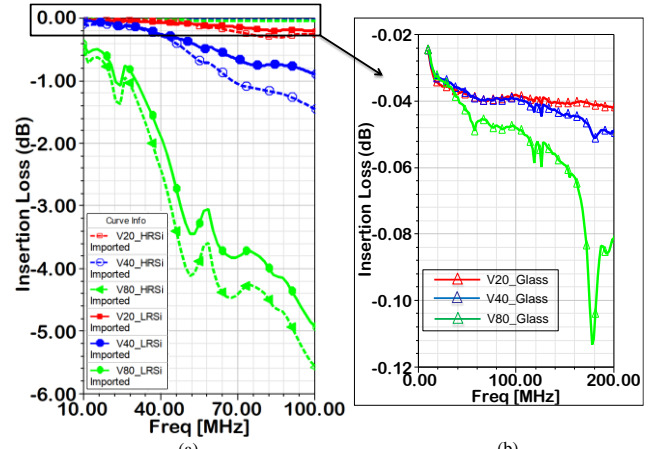


Fig.4. Variation in insertion loss performances (measurement) on low resistivity silicon (LRSi) substrate, high resistivity silicon (HRSi) substrate and on glass. (a) Full comparison. (b) Zoom around the glass insertion loss responses to show on-glass performances superiority.

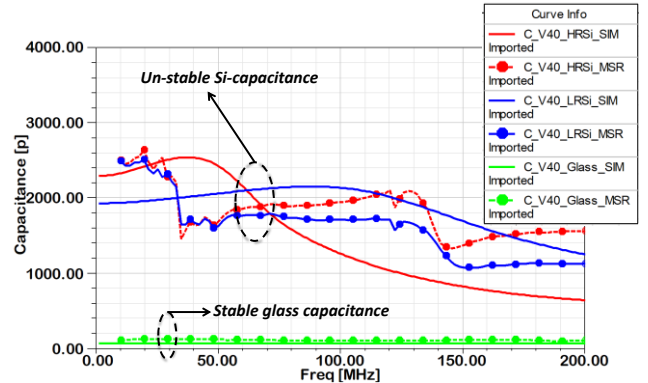


Fig.5. Comparison between extracted capacitance on simulation and measurement of ion-trap version V40_5 on HRSi, LRSi and glass respectively.

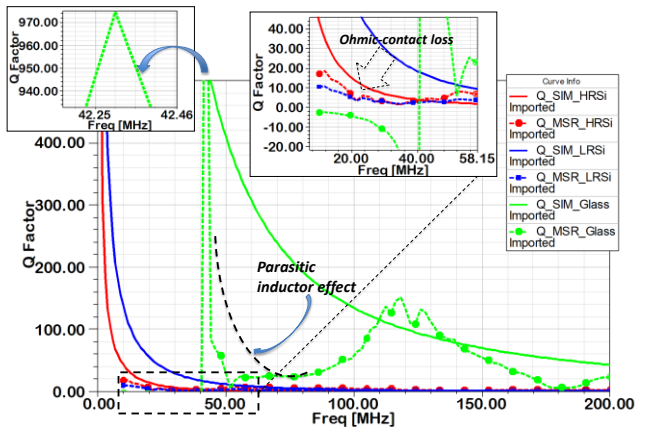


Fig.6. The comparison between simulation and probing measurement of ion-trap Q factor showing the Ohmic loss effect at frequency range below 50 MHz and effect of parasitic inductor to the measured Q factor of ion-trap on-glass.

capacitance value across the bandwidth of operation. When the capacitance is non-linear (un-stable) across the operating frequency, lower Q factor is produced. This can be translated to lower power spectral density and worse power efficiency.

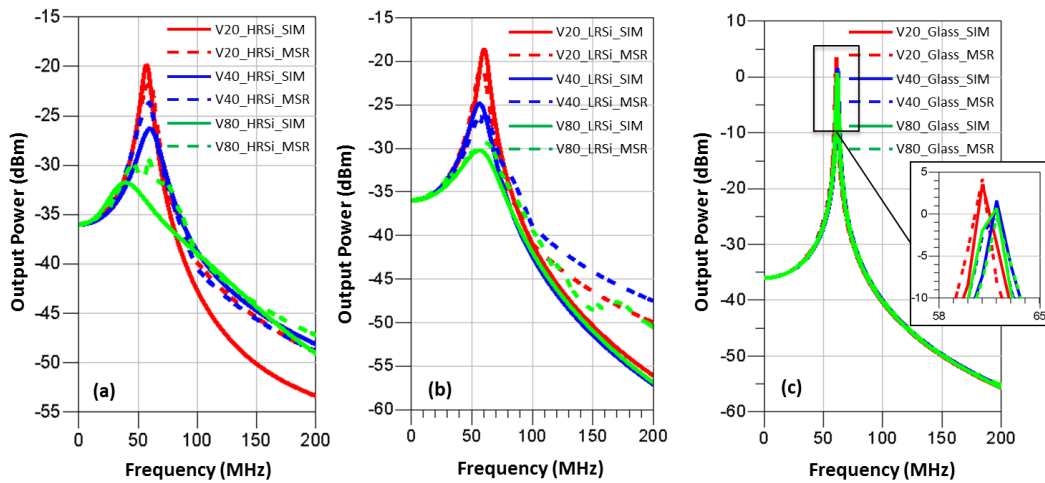


Fig.7. The resonance condition of ion-traps on three evaluated substrates (HRSi, LRSi, and glass) for the three variant of test vehicles (V20_5, V40_5, V80_5). (a) The resonance condition of ion traps on HRSi which show the comparison between simulation results (solid lines) and measurement results (dotted lines). (b) & (c) The resonance condition the counterpart on LRSi and glass respectively. In this case, the resonance peaks of HRSi and LRSi are around $-18 - 20$ dBm for V20_5, around -25 dBm for V40_5 and $-(30 - 32)$ dBm for V80_5. On another hand, the resonance peaks of ion-trap on-glass are about $1 - 4.2$ dBm.

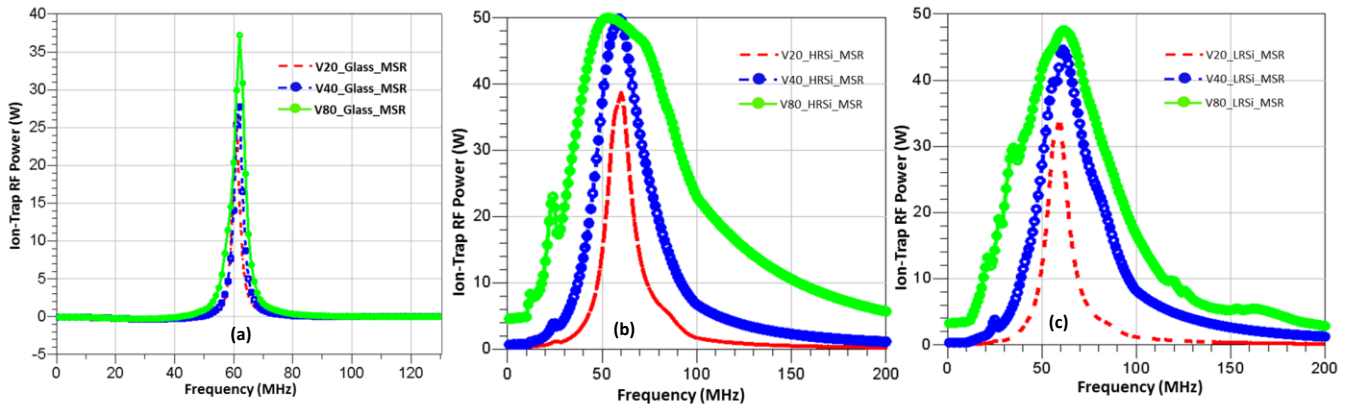


Fig.8. The ion-trap power spectral density measurement. (a) The ion-trap on-glass power spectral density due to 60 MHz RF input source excitation. (b) and (c) The respective power spectral density of ion-trap on HRSi and LRSi respectively.

So, non-linear Si capacitor behavior as shown by Fig.5 is undesirable effect in ion-trap design.

Capacitive devices exhibit Q factor responses profile in the form of hyperbolic curves. The existence of parasitic resistance and inductance will influence the shape of this hyperbolic curve. Series parasitic resistance will result in reduction of power resonance peak and broader bandwidth of power density, which can be translated to lower attainable Q factor. Hence, ion trap with longer RF line will have lower Q factor due to higher equivalent series resistance (ESR). During the measurement, the effect of series resistance can also be added by Ohmic contact-losses that are introduced by the physical contact between probing tips and the metallization surfaces of the ion-trap. The effect of the Ohmic contact-losses can be seen in Fig.6 at frequency below 50-MHz. In this case, the Ohmic contact-losses have significant effect to the Q factor of ion-trap on LRSi. This can be attributed to the low equivalent series resistance (around 5 - 15 Ohm) in the ion-trap on LRSi. So, the Ohmic-contact resistance around 10 Ohm will reduce its Q factor by factor of ~ 2 . On the other hand, this Ohmic-contact resistance only changes the equivalent resistance of HRSi (600 - 800-Ohm) by 8% - 10%, which results in proportional reduction on its Q factor.

The parasitic inductance may significantly alter the hyperbolic response shape of capacitor Q factor at certain frequency range depending on the bandwidth of the parasitic inductance. The Q factor of inductor is zero at DC and is gradually increasing with frequency. The effect of parasitic inductor can be seen in Fig.6 to the Q factor of ion-trap on-glass. In this case, ion-trap on-glass has measured peak Q factor equal to 974 at 42-MHz. Instead, it gradually decreases following the hyperbolic response curve as simulated; it drops sharply to value close to zero at 51MHz. From 51-MHz to 120MHz, the effect of parasitic inductance dominates the overall Q factor. From 120-MHz onward, the Q factor response of ion-trap on-glass shows the continuation of hyperbolic-curve response as in simulation.

B. Resonance Condition

Fig. 7(a)-(c) show the comparison between simulation and measurement results of output power responses of ion-trap test vehicles (V20_5, V40_5 and V80_5) on HRSi, LRSi and glass substrates respectively. The output resonance peaks of HRSi and LRSi (with the inclusion of Ohmic-contact loss in simulation) show close agreement between simulation and measurement results. These resonance peaks reflect the ion-

TABLE III
PERFORMANCE COMPARISON SUMMARY OF ION-TRAP CHARACTERIZATION ON HRSi, LRSi, AND GLASS.

Design Substrate	LRSi			HRSi			Glass		
	V20_5	V40_5	V80_5	V20_5	V40_5	V80_5	V20_5	V40_5	V80_5
Insertion loss (dB)	0.2	0.5	3.0	0.5	0.9	4.0	<0.1	<0.1	<0.1
Return loss (dB)	25	17	10	27	18	10	48	48	40
capacitance (pF) @60MHz	1200	2000	8000	1200	2000	3200	100	150	180
Q factor @60MHz	320	380	160	10	15	20	>900	>900	>900
Output power resonance peak (dBm)	-30	-25	-21	-30	-24	-20	5	1.8	1.7
Power Spectral Density									
P_{MAX} (W)	39	50	50	34	45	48	25	29.5	40
BW_{3dB} (MHz)	10.0	20	48	10.0	20.8	36	1.8	2.0	2.4
P_{3dB} (W)	27.6	35.35	35.35	24.04	31.8	33.94	17.68	20.85	28.28
PSD (W/MHz)	2.76	1.77	0.73	2.4	1.53	0.94	9.82	10.425	11.78

traps power efficiency at resonance frequency of 60MHz. In this case, ion-traps on-glass is 25 – 35 dBm more efficient than ion-traps on Si counterparts. As a consequence, ion-trap on Si substrate will have higher power dissipation, as small fraction of output power is used to form pseudopotential while the remaining power dissipates through the substrate forming stray E-field as illustrated in Fig. 2.

To give more insight about power efficiency, the power spectral densities of ion-traps are calculated based on s-parameter measurement. Power spectral density shows the delivered power into the ion-trap across the bandwidth of resonance. In this case, the 3dB-bandwidth will be used as a reference for the calculation of power spectral density (W/MHz). The power density calculations are summarized in Table 3. As given by Table 3, power spectral density of ion-trap on glass is far superior (9.8 – 11.8 W/MHz) than Si counterpart (only 0.8 – 2.8 W/MHz). As seen in Fig.7(c), ion-traps on-glass exhibit needle-like power density responses that show their efficiency in delivering power from source to the ion-trap metallization for current-to-E-field conversion. This can be correlated to strong E-field concentration around the trapping zone of ion-trap on-glass as illustrated by Fig.2(c).

Power spectral density also suggests the power dissipation outside the passband of frequency response. As seen in Fig. 8(a), the power is near to zero at frequency below 50MHz and above 80MHz of ion-trap on-glass frequency responses. This postulates that the power dissipation outside the PSD passband is near to zero Watt. On the other hand, ion-trap on HRSi and LRSi show power level of 24 – 35W outside their 3dB power bandwidth, which indicate ion-traps on Si substrate have significantly higher power dissipation than glass substrate. These can also be correlated to E-field distribution of ion-trap

on HRSi and LRSi which show large stray E-field density around the exposed (non-metallized) silicon area.

IV. MICROFABRICATION

The microfabrication of ion-traps on LRSi and HRSi are done in 300mm Si wafer platform as illustrated by Fig.9. First, the 3 μ m SiO₂ layer is formed by low-stress Plasma-Enhanced Chemical Vapor Deposition (PECVD). After patterning and dry etching of the insulation layer, 0.1 μ m Ti adhesion layer and 0.1 μ m Cu seed layer are subsequently deposited on top of the insulation layer. Next, 3.7 μ m Cu and 0.2 μ m Au layers are deposited by electrochemical plating (ECP) process. In the end, metal seed layer will be etched back to avoid shorts especially between RF and ground electrodes.

On the other hand, the microfabrication of the ion-trap on glass is more straightforward. Due to the use of glass substrate, the original insulation layer between silicon and metal electrodes can be eliminated. Adhesion layer and seed layer are directly deposited on the glass substrate. Same process as described above will be utilized for electrode patterning. However, to simplify seed layer etching process, a Cu layer with reduced thickness (2.5 μ m) is used.

The first challenge in microfabrication of the ion-traps is the leakage current that flow from one conductor to another via the substrate. Due to large applied peak-to-peak voltage (200V_{pp} – 250V_{pp}) into the RF electrodes, the leakage current will result in huge power dissipation. To minimize the leakage current, thick SiO₂ insulator layer is deposited on top of Si substrate. The use of high resistivity silicon substrate further minimizes the leakage current. Another challenge is on the etching of metal seed layer especially between RF and ground electrodes.

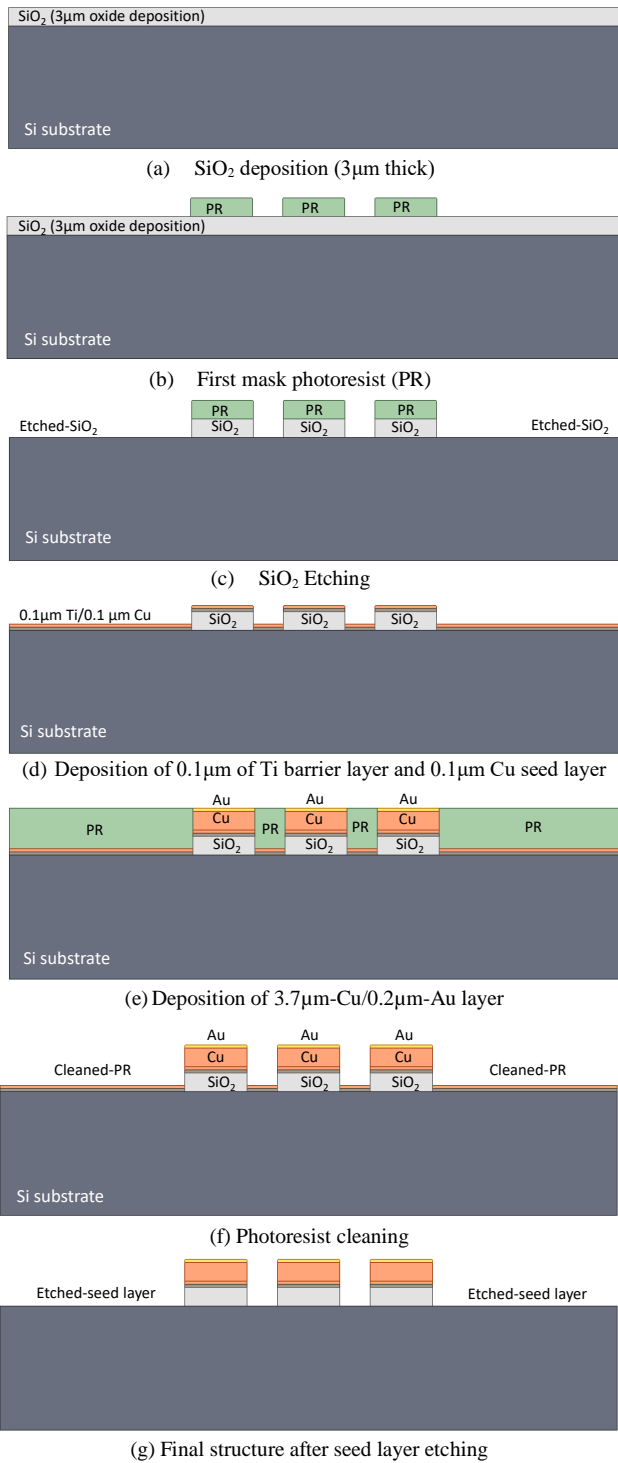


Fig.9. Microfabrication process schematic for ion-trap on silicon substrate (not to scale).

Fig. 10 shows the Cu seed residue remained in between the electrodes during the seed layer etching process. Narrow gap and high sidewall make it difficult for complete etching. Cu residue can be detected by applying low peak-to-peak RF signal (1 – 5V_{pp}) into the electrodes of the ion-traps and

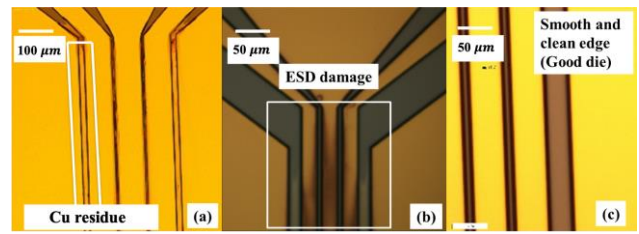


Fig. 10. Microfabrication of the ion-traps (top view): (a) Die with Cu residue. (b) ESD damage due to Cu residue upon application of RF voltage. (c) Smooth edge of good die.

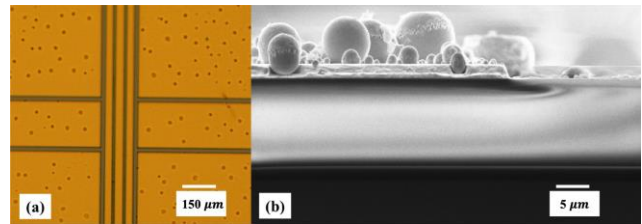


Fig.11. Cu oxidation issue. (a) Image from optical microscope. (b) SEM image.

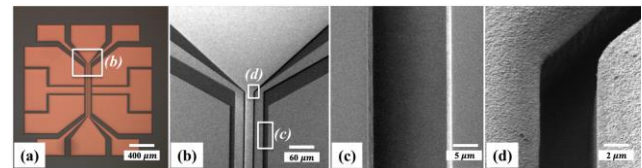


Fig.12. The structure of microfabrication of the ion-traps on Si substrate with detail zoom into the gap between electrodes.

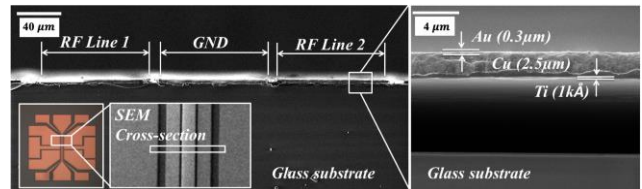


Fig.13. The structure of microfabrication of the ion-traps on glass substrate with detail zoom into the metallization thickness area.

observing their s-parameters (insertion loss, return loss and impedance characteristic) with respect to reference known-good part. In this case, the residue will affect insertion loss of the ion-trap and the amount of drop to insertion loss will depend on the amount of residue. Large Cu residue (as in Fig. 10(a)) can be visually inspected and cause large drop in insertion loss, that easily identifiable during the RF testing. However, little Cu residue may not significantly affect the insertion loss performance and can be undetectable during the RF testing. Despite insignificant effect in RF testing, little Cu residue possesses hidden threats in causing electro-static discharge (ESD) during ion-trap testing in ultra-vacuum environment when large peak-to-peak voltage (200V_{pp} – 250V_{pp}) is applied into the electrodes, as shown by Fig. 10(b). Therefore, it is essential to obtain smooth conductor edges for lower susceptibility to ESD. As ESD often occurs from the accumulation of concentrated charges in pointy (non-smooth) regions, smooth edges as shown in Fig. 10(c) is necessary to prevent ESD.

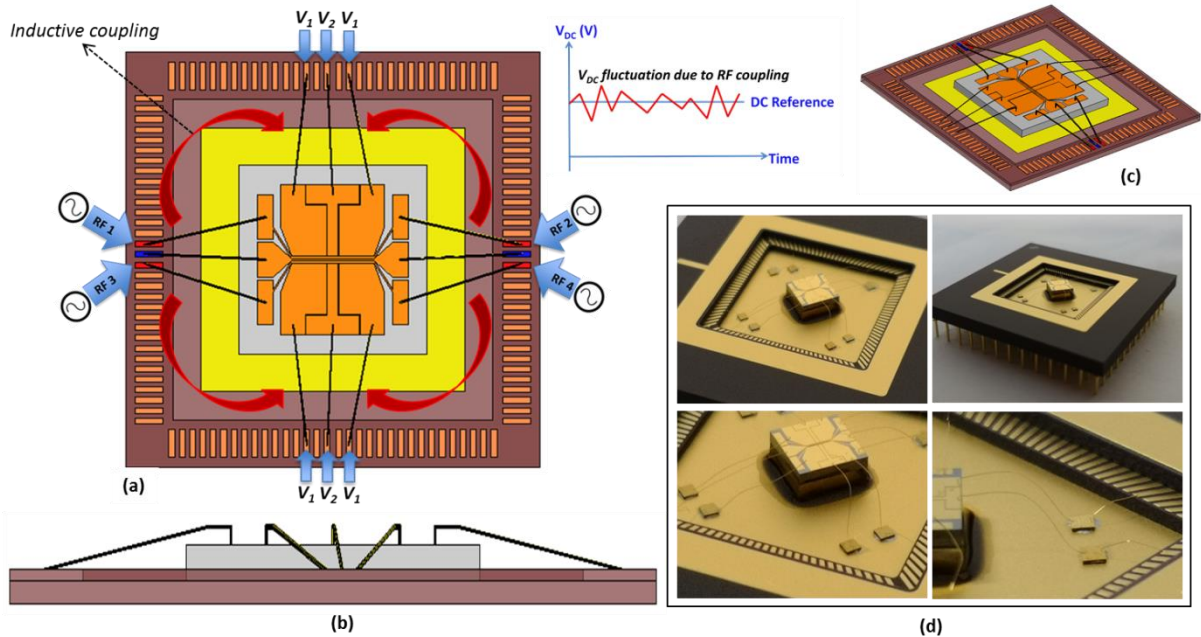


Fig. 14. Integration of ion-trap into CPGA packaging using bonding wire as interconnects. (a) Top view with RF and DC bias excitation. (b) Elevation view. (c) The bird-eye view. (d) Sample picture of final integration of ion-trap chip (V40_5) into CPGA packaging with bypass capacitor.

Copper can actively interact with oxygen to form cuprous oxide (Cu_2O) or cupric oxide (CuO), which affects the overall conductivity of copper. High surface roughness in copper may also increase the oxidation rate due to high surface area interaction. This oxidation issue on ion-trap metallization (as shown in Fig.11) reduces the strength of E -field due to the increase in resistivity of the copper surface. Hence, a thin layer of Au is deposited on top of copper layer to overcome this oxidation problem. Fig.12 and Fig.13 show the final microfabrication of surface electrode ion-traps on Si and on glass substrate respectively.

V. ON-PACKAGING PERFORMANCE

Fig.14 shows the modeling of ion-trap chip on CPGA packaging with bonding wire interconnections. The RF lines are excited by 200V peak-to-peak RF voltage. Such a high voltage swing can affect the DC biasing condition through inductive coupling via the bonding wires. Change in DC biasing condition may affect the axial confinement and ion position may shift accordingly along the ground line axis. This will increase the complexity of ion addressing since laser spatial accuracy of ten-to-hundreds of nm is needed. To minimize the inductive coupling from RF bonding wires to DC wires, the RF excitation and DC biasing set-up are orthogonally connected to side pins of CPGA packaging to minimize cross-talk.

Fig.15 shows the measured output power resonance condition (dBm) of ion-trap chips on CPGA packaging. To avoid excessive power injected into the oscilloscope, capacitive power divider of $C_1:C_2 = 1:20$ is used. Hence, the peak output powers are about 20 – 20dBm lower than calculated values as given by Fig.7. Some discrepancies on the peaks of output power resonances are found, which can be attributed to cable losses and capacitor losses. The cables

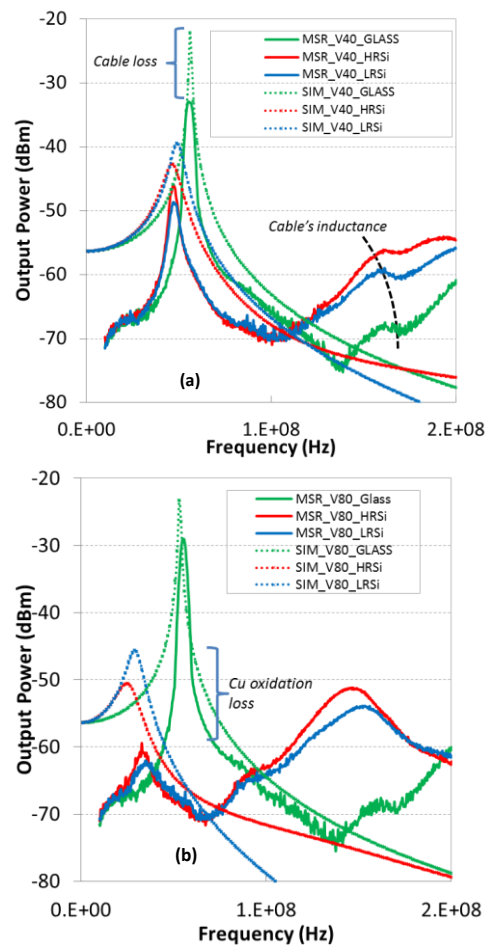


Fig.15. Comparison between simulation and measurement of output power of ion-trap chips on CPGA packaging with bonding wires interconnects. (a) Output power of V40_5. (b) Output power of V80_5.

that connect the packaging into the resonator box are not taken into account. On the other hand, the cables parasitic inductance affects the fly-back resonance condition at frequency higher than 100MHz. The discrepancies between simulation and measurement results of V80_5 ion-trap chips are higher, which may be due to the copper oxidation that is mostly found on the bigger version of ion-trap test vehicles.

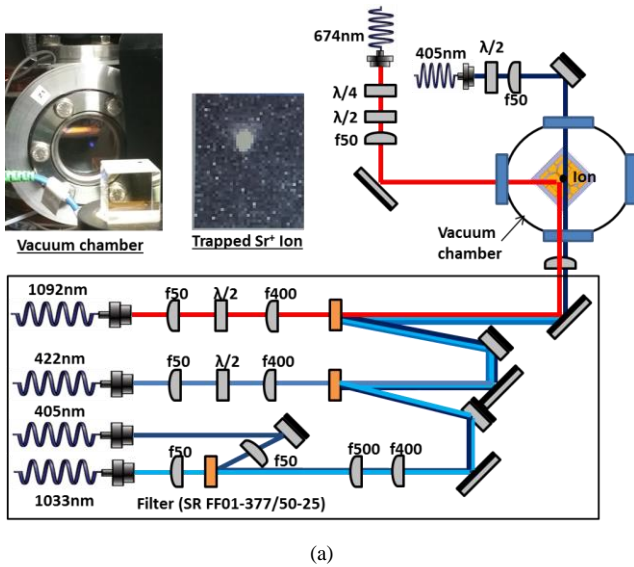


Fig.16: (a) Laser system optical set-up for Qubit operation (674nm), Doppler cooling and detection (422nm), re-pumping (1033 and 1092nm) and ionization (405nm). (b) Ion-laser interaction in $^{88}\text{Sr}^+$ ion for electron ground-state ($5s^2S_{1/2}$) and excited state ($4d^2D_{5/2}$) transition (quantum logic $|0\rangle$ to $|1\rangle$ transition) [21].

VI. ION-TRAP TESTING

Fig. 16(a) shows the laser optical set-up which successfully captures an $^{88}\text{Sr}^+$ ion for single qubit quantum operation. $^{88}\text{Sr}^+$ is used as the targeted ion qubit in this work due to its simple level structure and the availability of laser diodes for all relevant atomic transitions [21], [22]. For quantum computing operation in $^{88}\text{Sr}^+$ ion, 422nm, 674nm, 1033nm and 1092 nm lasers are used to induce the laser-atom interactions for inter-state transitions, as shown in Fig.16 (b) [23]. Fundamentally,

three primary steps are involved in quantum computing operation: (1) state initialization, (2) state transition, and (3) state detection [24]. The 422nm laser is used for state initialization to perform Doppler cooling on $^{88}\text{Sr}^+$ ion. Besides Doppler cooling, sideband cooling is also performed using 674nm laser to reach the motional ground state (or $|0\rangle$ state) of the $^{88}\text{Sr}^+$. After initialization state of ion qubit, state transition shall be performed. In addition to sideband cooling, 674nm clock transition laser is also used for $|0\rangle$ to $|1\rangle$ state transition ($S_{1/2}$ to $D_{5/2}$ orbital transition). $D_{5/2}$ is selected as the $|1\rangle$ state due to its relatively long ($\sim 0.35\text{s}$) lifetime. Meanwhile, for $|1\rangle$ to $|0\rangle$ state transition, 1033 nm clear-out laser is used in driving the $D_{5/2}$ to $P_{3/2}$ orbital transition, which will be spontaneously decay to $S_{1/2}$ orbital, or ($|0\rangle$ state) due to short lifetime in $P_{3/2}$ orbital, as shown in Fig.16(b). A coherent superposition of the S and D states, $D_{3/2}$ is known as the Dark State which will hinder state transitions in $^{88}\text{Sr}^+$ ion. Therefore, the $D_{3/2}$ state needs to be continuously re-pumped to maintain cooling using 1092nm re-pumping laser [25], [26]. For state detection, the electron shelving technique is used to distinguish the S and D states, which corresponds to $|0\rangle$ and $|1\rangle$ states. The S state is coupled to the P state with a strong transition, which is continuously driven with the Doppler cooling laser at 422nm. If the ion is in the S state, photons are scattered and the ion fluorescence can be detected. If the ion is in the D state, no fluorescence is detected [25]. Thus, besides Doppler cooling, 422nm laser can also be used for S/D states detection.

VII. CONCLUSION

The ion-trap on-glass was tested to exhibit superior performance than ion-trap on-silicon in all design consideration parameters (insertion loss, Q factor, capacitance stability, power efficiency, power spectral density, and E-field density). In particular, glass ion-trap was tested to have significantly higher Q factor than its silicon counterparts. Such high Q factor leads to higher power efficiency and power spectral density (PSD). Glass ion-trap was also proven to have superior insertion loss performance. Due to its lossless properties, glass substrate was demonstrated to have low of stray E-field on the exposed surface (non-metallized area) but very high E-field density around trapping zone. Glass ion-trap was showed to have a more stable and linear equivalent capacitance, which gave more efficient current-to-E-field transformation. Based on the obtained results, the microfabrication structures were demonstrated to perform the ion-trapping functionality as simulated. With the success of capturing the $^{88}\text{Sr}^+$ ion, the laser system optical set-up was verified to perform the basic steps for quantum computing operation. In summary, the reported design and development procedure had been demonstrated to show the single qubit ion-traps functionality for quantum computing system.

REFERENCES

- [1] M. Kroner, M. Debatin, J. Mikosch, S. Trippel, E. Just, M. Reetz-Lamour, R. Wester, M. Weidemuller, P. Woias, "Simulation, Design and Test of a Novel Planar RF Micro Ion Trap," *TRANSDUCERS 2007 - 2007 International Solid-State Sensors, Actuators and Microsystems Conference*, Lyon, 2007, pp. 1665-1668 [10].

[2] A. Shorey, J. Keech, G. Piech, B. Wang and L. Tsai, "Glass substrates for carrier and interposer applications and associated metrology solutions," *ASMC 2013 SEMI Advanced Semiconductor Manufacturing Conference*, Saratoga Springs, NY, 2013, pp. 142-147.

[3] S. Takahashi, K. Horiuchi, S. Mori, K. Tatsukoshi, M. Ono, M. Mikayama, N. Imajo, T. Moble, "Development of through glass via technology for 3D packaging," *2013 European Microelectronics Packaging Conference (EMPC)*, Grenoble, 2013, pp. 1-4.

[4] M. Grabowski and W. Jablonski, "The technology of hard glass layers on silicon substrates and their application in microwave semiconductor devices," *ASDAM '98. Conference Proceedings. Second International Conference on Advanced Semiconductor Devices and Microsystems (Cat. No.98EX172)*, Smolenice Castle, Slovakia, 1998, pp. 103-106.

[5] J. Britton, D. Leibfried, J. A. Beall, R. B. Blakestad, J. H. Wesenberg, and D. J. Wineland, "Scalable arrays of rf Paul traps in degenerate Si," *Appl. Phys. Lett.*, vol. 95, 173102, Oct. 2009.

[6] D. Leibfried, R. Blatt, C. Monroe, and D. Wineland, "Quantum dynamics of single trapped ions," *Rev. Mod. Phys.*, vol. 75, pp. 281-324, Jan. 2003.

[7] P. See, G. Wilpers, P. Gill and A. G. Sinclair, "Fabrication of a Monolithic Array of Three Dimensional Si-based Ion Traps," in *Journal of Microelectromechanical Systems*, vol. 22, no. 5, pp. 1180-1189, Oct. 2013.

[8] S. Hong, Y. Kwon, C. Jung, M. Lee, T. Kim and D. D. Cho, "A New Microfabrication Method for Ion-Trap Chips That Reduces Exposure of Dielectric Surfaces to Trapped Ions," in *Journal of Microelectromechanical Systems*, vol. 27, no. 1, pp. 28-30, Feb. 2018.

[9] J. Wang, S. Paesani, Y. Ding, R. Santagati, P. Skrzypczyk, A. Salavrakos, J. Tura, R. Augusiak, L. Mančinska, D. Bacco, D. Bonneau, J. Silverstone, Q. Gong, A. Acín, K. Rottwitz, L. Oxenlowe, J. O'Brien, A. Laing, and M. Thompson, "Large-scale Integration of Multidimensional Quantum Photonics Circuits on Silicon," *2018 Conference on Lasers and Electro-Optics (CLEO)*, San Jose, CA, 2018, pp. 1-2.

[10] M. Y. Simmons, "Quantum computing in silicon," *2015 IEEE International Electron Devices Meeting (IEDM)*, Washington, DC, 2015, pp. 1.2.1-1.2.4.

[11] J. M. Amini, H. Uys, J. H. Wesenberg, S. Seidelin, J. Britton, J. J. Bollinger, D. Leibfried, C. Ospelkaus, A. P. VanDevender and D. J. Wineland, "Toward scalable ion traps for quantum information processing," *New Journal of Physics*, Volume 12, March 2010.

[12] K. K. Mehta, A. M. Eltony, C. D. Bruzewicz, I. L. Chuang, R. J. Ram, J. M. Sage and J. Chiaverini, "Ion traps fabricated in a CMOS foundry," *Applied Physics Letters*. 105. 10.1063/1.4892061.

[13] D. Stick, W. K. Hensinger, S. Olmschenk, M. J. Madsen, K. Schwab and C. Monroe, "Ion trap in a semiconductor chip," *Nature Physics* 2, 36-39 (2005)

[14] S. X. Wang, Y. Ge¹, J. Labaziewicz, E. Dauler, K. Berggren, and I. L. Chuang, "Superconducting microfabricated ion traps," *Appl. Phys. Lett.* 97, 244102 (2010)

[15] S. C. Doret, J. M. Amini, K. Wright, C. Volin, T. Killian, A. Ozakin, D. Denison, H. Hayden, C.-S. Pai, R. E. Slusher, "Controlling trapping potentials and stray electric fields in a microfabricated ion trap through design and compensation," *New Journal of Physics*, Volume 14, July 2012

[16] D. T. C. Allcock, J. A. Sherman, D. N. Stacey, A. H. Burrell, M. J. Curtis, G. Imreh, N. M. Linke, D. J. Szwer, S. C. Webster, A. M. Steane and D. M. Lucas, "Implementation of a symmetric surface-electrode ion trap with field compensation using a modulated Raman effect," *New Journal of Physics*, Volume 12, May 2010.

[17] S. Hong, M. Lee, H. Cheon, J. Ahn, M. Kim, T. Kim, D. D. Cho, "New scalable microfabrication method for surface ion traps and experimental results with trapped ions," *2015 28th IEEE International Conference on Micro Electro Mechanical Systems (MEMS)*, Estoril, 2015, pp. 292-295

[18] J. Tao, N. P. Chew, L. Guidoni, Y. D. Lim, P. Zhao and C. S. Tan, "Fabrication and Characterization of Surface Electrode Ion Trap for Quantum Computing," *2018 IEEE 20th Electronics Packaging Technology Conference (EPTC)*, Singapore, Singapore, 2018, pp. 363-366.

[19] J. Wesenberg, "Electrostatics of surface-electrode ion traps," *Phys. Rev. A* 78,063410 (2008).

[20] D. Gandolfi, M. Niedermayr, M. Kumph, M. Brownnutt, and R. Blatt, "Compact radio-frequency resonator for cryogenic ion traps," *The Review of scientific instruments*. 83. 084705. 10.1063/1.4737889.

[21] S. X. Wang, "Quantum gates, sensors, and systems with trapped ions," Massachusetts Institute of Technology, 2012.

[22] "Large two dimensional Coulomb crystals in a radio frequency surface ion trap," *Appl. Phys. Lett.*, vol. 100, no. 17, 2012.

[23] C. D. Bruzewicz, J. Chiaverini, R. McConnell, and J. M. Sage, "Trapped-ion quantum computing: Progress and challenges," *Appl. Phys. Rev.*, vol. 6, no. 2, 2019.

[24] J. P. Likforman, V. Tugayé, S. Guibal, and L. Guidoni, "Precision measurement of the branching fractions of the 5p P1/2 2 state in Sr + 88 with a single ion in a microfabricated surface trap," *Phys. Rev. A*, vol. 93, no. 5, pp. 1-21, 2016.

[25] G. Higgins *et al.*, "Single Strontium Rydberg Ion Confined in a Paul Trap," *Physical Rev. X*, vol. 021038, pp. 1-11, 2017.

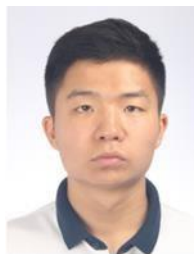
[26] M. G. House, "Analytic model for electrostatic fields in surface-electrode ion traps," *Phys. Rev. A - At. Mol. Opt. Phys.*, vol. 78, no. 3, pp. 1-8, 2008.



Anak Agung Alit Apriyana received the B.Eng and M.Phil degree from the Nanyang Technological University (NTU), Singapore, in 2003 and 2004 respectively, majoring in RF circuit design, and the Ph.D. degree from NTU in 2015. He worked at TDK-EPCOS Pte Ltd., Singapore, for five years as a Senior Product Development Engineer. He was in charge of the design and development of radio frequency integrated circuit surface acoustic wave (RF IC SAW) filters. He then joined NTU since January 2010, as a Researcher at the Virtus IC Design Centre, while pursuing his P.D. degree under IC design scholarship by the Economic Development Board of Singapore.



Hongyu Li received the Ph.D. degree in semiconductor physics and devices from the Changchun Institute of Physics, Chinese Academy of Science, China, in 1999. She is working on the process integration and reliability improvement for 3-D through-silicon-via (TSV) technology, wafer level Cu/Cu hybrid bonding and surface ion trap, as a senior scientist in the Institute of Microelectronics, Agency for Science, Technology and Research, Singapore. She has published more than 50 research papers and 5 Patents.



Peng Zhao (S'2020) received his B.E. degree in mechanical and material engineering from Tianjin University, Tianjin, China, in 2018. He is currently working toward the Ph.D. degree at Nanyang Technological University, Singapore. His Ph.D. focus area is design, modelling and characterization of surface electrode ion trap integrated

with TSV and photonic devices.



Jing Tao received the B.Eng. degree in measurement and control technique and instrument from Northwestern Polytechnical University, China, in 2006, and the M.Eng. degree in electronics engineering and information technology from the University of Applied Science

Deggendorf, Germany, in 2008. She worked as product quality engineer in Zollner Electronic, China, from 2008 to 2011. Then she began her doctoral work in Tyndall National Institute, University College Cork, Ireland and received her Ph.D. degree in microelectronics in 2016. She is currently a research fellow at Nanyang Technological University. Her current research interests include surface ion trap technology for quantum computing, TSV technology and 3D system integration.



Chuan Seng Tan (M'2007 – SM'2019) received his BEng degree in electrical engineering from University of Malaya, Malaysia, in 1999 and MEng degree in advanced materials from the National University in 2001. He then joined the Institute of Microelectronics, Singapore, as a research engineer. In the fall of 2001, he began his doctoral work

at the Massachusetts Institute of Technology, Cambridge, USA, and was awarded a Ph.D. degree in electrical engineering in 2006. He is currently a tenured full professor in NTU. His research interests are semiconductor process technology and device physics. Currently he is working on 3D packaging and integration. He is a recipient of the 2019 Exceptional Technical Achievement Award from the IEEE Electronics Packaging Society (EPS). He is a Fellow of the International Microelectronics Assembly and Packaging Society (IMAPS) since 2019.



Yu Dian Lim received the B. Eng. in Materials and M. Sc. of Materials Engineering from University of Malaya (UM), Malaysia, in 2011 and 2014, respectively. After that, he received the PhD in EEE from Nanyang Technological University (NTU), Singapore in 2018. He is currently holding a postdoctoral research fellow

position in School of Electrical and Electronic Engineering, NTU. He has involved in multidisciplinary researches, including nanomaterials, MEMS fabrication, communication device design etc. His current research interests include silicon photonics integrated circuit design and quantum computing.



Ye Lin (S'16-M'19) received his B.S. degree (2013) and Ph.D. (2019) from the School of Electrical and Electronic Engineering, Nanyang Technological University (NTU), Singapore. His research interests are integrated passive devices and 3-D integrated circuits.



Luca Guidoni received the Ph.D. degree at Pierre et Marie Curie University Paris, France, in 1998. He currently holds a CNRS researcher position at the MPQ laboratory of the Denis Diderot University in Paris. His research activity is mainly devoted to the experimental aspects of light-matter interaction with a particular interest in

quantum optics and laser cooling of atoms and ions.